Hyperspectral Classification Through Unmixing Abundance Maps Addressing Spectral Variability

Edurne Ibarrola-Ulzurrun, Lucas Drumetz, *Member, IEEE*, Javier Marcello, *Senior Member, IEEE*, Consuelo Gonzalo-Martín, and Jocelyn Chanussot, *Fellow, IEEE*

Abstract—Climate change and anthropogenic pressure are causing an indisputable decline in biodiversity; therefore, the need of environmental knowledge is important to develop the appropriate management plans. In this context, remote sensing and, specifically, hyperspectral imagery (HSI) can contribute to the generation of vegetation maps for ecosystem monitoring. To properly obtain such information and to address the mixed pixels inconvenience, the richness of the hyperspectral data allows the application of unmixing techniques. In this sense, a problem found by the traditional linear mixing model (LMM), a fully constrained least squared unmixing (FCLSU), is the lack of ability to account for spectral variability. This paper focuses on assessing the performance of different spectral unmixing models depending on the quality and quantity of endmembers. A complex mountainous ecosystem with high spectral changes was selected. Specifically, FCLSU and 3 approaches, which consider the spectral variability, were studied: scaled constrained least squares unmixing (SCLSU), Extended LMM (ELMM) and Robust ELMM (RELMM). The analysis includes two study cases: 1) robust endmembers and 2) nonrobust endmembers. Performances were computed using the reconstructed root-mean-square error (RMSE) and classification maps taking the abundances maps as inputs. It was demonstrated that advanced unmixing techniques are needed to address the spectral variability to get accurate abundances estimations. RELMM obtained excellent RMSE values and accurate classification maps with very little knowledge of the scene and minimum effort in the selection of endmembers, avoiding the curse of dimensionality problem found in HSI.

Index Terms—CASI, hyperspectral image classification, spectral unmixing, Hughes phenomenon, endmembers, spectral variability.

I. INTRODUCTION

DURING the past decades, the increasing loss of biodiversity has become a global concern [1]. For instance, variations in vegetation lead to an alteration of the habitat structure, causing the changes in the ecosystem biodiversity. Thus, knowledge on the conservation status and habitat structure of natural areas becomes essential for environmental management. Nowadays, most conservation status assessments are based on field observations and/or aerial photo interpretations, being a very labor-intensive process and a time-consuming process. Instead, remote sensing is a valuable, accurate, and repeatable tool for mapping and monitoring ecosystems and to study their conservation status [2], [3]. Specifically, hyperspectral image analysis techniques have significantly contributed to these tasks. However, it remains a challenge, requiring sensors and methods that can deal with complex habitats structures present in ecosystems [1], [4].

Hyperspectral imagery (HSI) is built by hundreds of narrow and contiguous spectral bands covering the electromagnetic spectrum, typically from the visible to the near-infrared, and sometimes also shortwave infrared spectral bands (0.3–2.5 μm) [5], [6]. The rich spectral information available in HSI increases the capability of precisely discriminating the materials or covers of interest [7], [8].

Hyperspectral image classification has been a very active area of research in the lpast years [9], [10]. Even though HSI is a suitable tool for source separation and classification processes, conventional HSI classification methods suffer from important limitations for detailed ecosystem mapping due to the limited degree of detail that can be mapped. It also increases the computational load because of the enhancement of spectral resolution, which leads to high-dimensional data that can degrade the classification process [11]. Another limitation of HSI classification is the little availability of the ground truth data in practice. For instance, supervised classification is generally a difficult task due to the ratio between the high dimensionality of the data and the limited availability of labeled training samples [7]. The rule of thumb is that

E. Ibarrola-Ulzurrun is with the Instituto de Oceanografía y Cambio Global, Universidad de Las Palmas de Gran Canaria, 35100 Las Palmas, Spain (e-mail: edurne.ibarrola101@alu.ulpgc.es).

L. Drumetz is with IMT Atlantique, Lab-STICC, UBL, 29238 Brest, France (e-mail: lucas.drumetz@imt-atlantique.fr).

J. Marcello is with the Instituto de Oceanografía y Cambio Global (IOCAG), Universidad de Las Palmas de Gran Canaria (ULPGC), Parque Científico Tecnológico Marino de Taliarte, 35100 Las Palmas, Spain (e-mail: javier.marcello@ulpgc.es).

C. Gonzalo-Martín is with the Department of Computer Architecture and Technology, Universidad Politécnica de Madrid, Campus de Montegancedo, 28660 Madrid, Spain (e-mail: chelo@fi.upm.es).

J. Chanussot is with the Grenoble Images Speech Signals and Automatics Laboratory (GIPSA-Lab), Grenoble Institute of Engineering, CNRS, University of Grenoble Alpes, 38000 Grenoble, France (e-mail: jocelyn.chanussot@gipsa-lab.grenoble-inp.fr).

Color versions of one or more of the figures in this paper are available online at http://ieeexplore.ieee.org.

Digital Object Identifier 10.1109/TGRS.2019.2892903

the required number of training samples is linearly related to the dimensionality of the data. This problem is called the *curse of dimensionality* or *Hughes phenomenon* [10], [12], which specifies that the size of training samples set required for classification increases exponentially with the number of spectral bands [13].

On the other hand, when more details are required in the classification process, the more difficulties arise, such as *mixed pixels*, leading to lower accuracy in classification maps [2]. In addition, the spatial resolution of a sensor could be too low to distinguish materials, leading to a composite of individual spectra in the same pixel. Thus, the recognition of pixels is frequently a combination of numerous materials, which introduces a need to quantitatively decompose, or *unmix*, this mixture [14]. In this context, hyperspectral unmixing may be the right tool to move beyond the pixel-based limitations for ecosystem mapping and monitoring [2].

Spectral unmixing refers to any process that retrieves the pure spectral components, called *endmembers*, and a set of fractional *abundances*, which indicate the proportion of each endmember [7], [14]. Endmembers are, generally, assumed to represent the pure materials present in the image, whereas the set of abundances at each pixel represents the percentage of each endmember present in the pixel [5], [7]. The potential of spectral unmixing to estimate the spatial distribution and abundances of invasive species and vegetation has been studied [2], [15]–[17]. Thus, spectral unmixing could be a suitable methodology for environmental management. However, there are some issues found in unmixing techniques: 1) the notion of a pure material can be subjective and problem dependent, hence leading to a definition of endmembers that depends on the application and spatial resolution [5] and 2) most studies assume that a proportion represents the percentage of material associated with an endmember present in a pixel. However, Hapke [18] states that the abundances in a linear mixture represent the relative area of the corresponding endmembers in a pixel [5].

Unmixing models can be, either, linear or nonlinear [5]. In most applications, the linear mixing model (LMM) is assumed considering that contributions of each endmember sum up in a linear way [5]. According to the LMM definition, data lie into a simplex whose vertices are defined by the endmembers [19]. However, LMM is not accurate since many real physical processes are inherently nonlinear, e.g., multiple scattering and intimate mixing, contribute to the measured radiance or reflectance. The most important source of the error in LMM lies in the lack of ability to account for sufficient temporal and spatial spectral variability. This can result in significant estimation errors being propagated throughout the unmixing process [6], [20]–[22].

This paper focuses on spectral unmixing models in which the spectral variability is considered, as well as the spatial information. The main objectives can be divided into the following.

1) *Analysis of the Endmember Variability:* The endmember spectral signature can change depending on the geometry and topography of the scene, atmospheric effects, and noise in the image or variation in a hidden parameter (e.g., water content in vegetation). Considering endmember variability, a significant improvement can be achieved.
2) Analysis of the use of classification maps to assess the performance of the unmixing models.
3) Obtaining accurate classification maps in a mountainous ecosystem with high spectral variability using few training samples, solving the issues caused by the hyperdimensionality of the data.

In this context, different unmixing models are evaluated: 1) fully constrained least squares unmixing (FCLSU), a traditional LMM; 2) scaled constrained least squares unmixing (SCLSU) approach [19], [23]; 3) extended LMM (ELMM) that extends the LMM by considering endmember variability while preserving the LMM framework, and allowing the pixelwise variation of the endmembers according to scaling factors [19], [24]; and finally 4) robust ELMM (RELMM) [25], a refined formulation of ELMM. The effects of the endmembers' purity and quantity for each class are also analyzed. Accurate classification maps are obtained, taking the abundance maps as inputs, to avoid the *Hughes phenomenon*, and using a hard classification method.

This paper is structured as follows. Section II contains the study area and the description of the data sets. Section III presents the analyzed unmixing algorithms. Section IV describes the applied methodology. Section V includes the main results and a critical analysis. Finally, Section VI summarizes the main outcomes and contributions.

II. STUDY AREA

The study is focused on a volcanic vulnerable and heterogenic ecosystem of Tenerife island (Canary Islands, Spain), the Teide National Park (28° 06' N 15° 24' W). The climate of the National Park is conditioned by the extreme altitude conditions (ranging between 2000 and 3718 m), strong insolation, and thermal variations. It can be defined as a subalpine continental climate, very different from the prevailing one in the low and middle areas of the island [26]. It is a remarkable biodiversity hotspot with high variability of endemic species vulnerable to environmental changes [27], making Teide National Park an ecosystem with a high interest of study from an ecological point of view. The discrimination of the heterogeneous vegetation communities found in the study area is a challenging task because different vegetation may have similar spectral response and even the same plant species has phenological changes depending on its location in the Park. In addition, due to the climate change and the increment of the European rabbit population, *Spartocytisus supranubius*, a very important species in the Teide National Park, is showing a negative density damage, leading to an absence of rejuvenation, while *Pterocephalus lasiospermus* has increased its distribution and abundance despite the presence of a nonnative generalist herbivore [28]. For these reasons, it is important to carry out a detailed study of the Teide National Park in order to develop a suitable management plan by the managers of the Park.

The nonherbaceous vegetation species, selected for the study due to their abundance and importance at the ecological
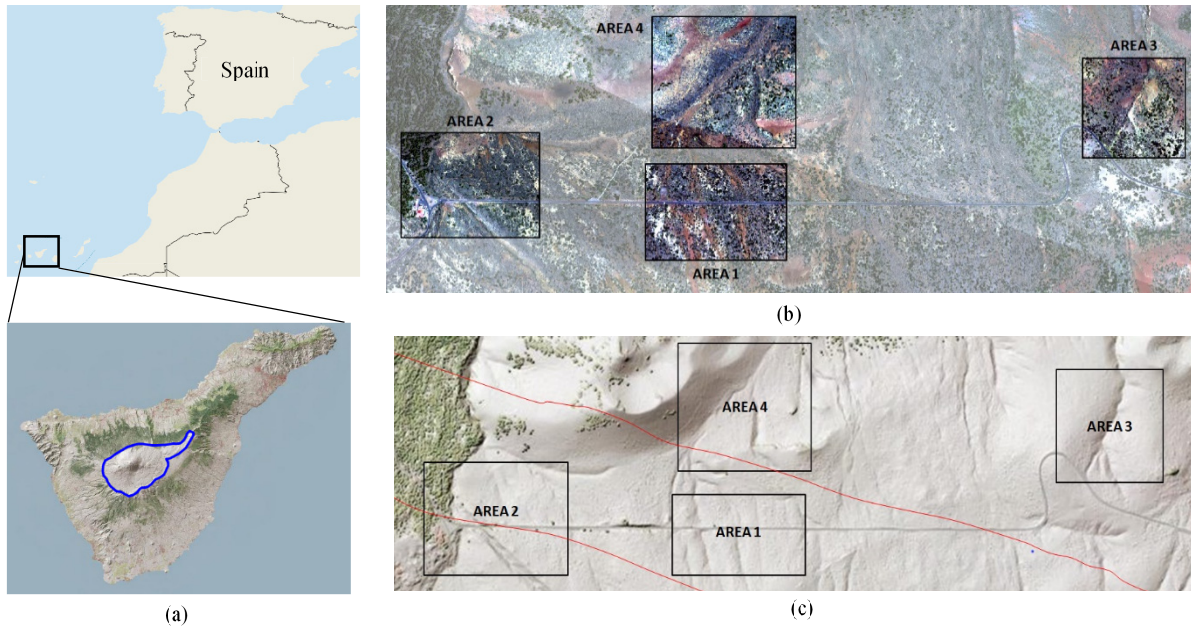
Fig. 1.   Teide National Park. (a) Geographic location. (b) True color composite (CASI bands X, Y, and Z nm) highlighting the four subsets used in the study. (c) Digital elevation model and the swath limits in red.

level, were: *Pinus canariensis*, *Spartocytisus supranubius*, *Pterocephalus lasiospermus*, and *Descurainia bourgaeana*. The period of the year was an important factor in the selection of the acquisitions, since the relevant species bloom during spring and species are at their greatest point of spectral difference. However, plant individuals do not bloom at the same time in every part of the study area, due to climatic differences through the Park, leading to an additional spectral variation within the same plant species.

In this context, the image used for this study was acquired on June 1, 2017 through the Compact Airborne Spectrographic Imagery (CASI) sensor configured with 68 spectral bands, covering a range from 0.3969 to 1.0390 μm and a spatial resolution of 0.75 m. It was radiometrically and atmospherically corrected as well as georeferenced (Product Level 2c) [29]. Four different subsets (Fig. 1) were selected to evaluate the algorithms in an image with spectral variability related to the topography changes due to the mountainous ecosystem (Areas 3 and 4) and radiometric changes between different swaths that appear when acquiring the CASI imagery (Areas 2 and 4). Area 1 was chosen as a control subset in a zone without either topographic or radiometric changes. Finally, the four subsets have another intrinsic spectral variability due to the blooming of plant individuals.

III. UNMIXING ALGORITHMS

A. Linear Mixing Model

Several studies have investigated the mixing scales and linearity. Singer and McCord [30] found that if the scale of the mixing is large (macroscopic), mixing occurs in a linear fashion. For microscopic or intimate mixture, the mixing is generally nonlinear [30], [31]. The LMM assumes no interaction within materials: the incident light interacts with just one material [5]. LMM considers a linear combination of the pure spectral of the materials located in the pixel area, weighted by their fractional abundance (1). P is the number of endmembers considered, s_p is a reference endmember providing the direction of a straight line joining the origin at that point on which each local endmember lies, a_{pn} is the abundance coefficient of the endmember in pixel n, e_n is the additive noise

$$x_n = \sum_{p=1}^{P} a_{pn} s_p + e_n. \tag{1}$$

However, LMM shows some limitations such as nonlinearities in the mixing processes and material variability. Endmember variability comprehends that each material cannot be completely represented by a single spectrum, being a subject of intraclass variations [20]. Traditional FCLSU [32] has been used in this paper.

In the literature, endmember variability has been addressed using endmember bundles [33], which incorporate variability by representing each endmember by a set of spectra, each of which could reasonably be the reflectance of an instance of the endmember. Thus, endmember unmixing needs to be extended to bundle unmixing and using multiple signatures for each endmember class may provide more accurate fractions [34], [35]. In this context, several studies have implemented different methods, which deal with the endmember spectral variability, such as multiple endmember spectral mixture analysis (MESMA) [36], AutoMCU [37], and perturbed LMM (PLMM) algorithm [6].

B. Scaled Constrained Least Squares Unmixing

The SCLSU (2) model is based on LMM. It uses the non-negative least squares to estimate the spectral variability [19],

[23]. ψ_k is added as a scaling factor considering the brightness changes in the spectral signature of a pixel

$$x_n = \psi_k \sum_{p=1}^{P} a_{pn} s_p + e_n. \qquad (2)$$

Yet, SCLSU cannot consider other types of variability than scaling factors. It is a simple approach to address spectral variability assuming a scaling factor that affects equally to all the endmembers present in a pixel. Thus, a more complex version was proposed, the ELMM, which is next described.

C. Extended Linear Mixing Model

Spectral variability can be modeled using an accurate radiative transfer-based model such as the Hapke model [18]. This physical model allows accessing the reflectance value of a material for one wavelength, knowing the corresponding single scattering albedo, the photometric parameters of the material, and the incidence, emergence, and azimuth angles during the acquisition. ELMM was derived from this model using simplifying physical assumptions [38]. ELMM [19], [24] allows a pixelwise variation of each endmember (the code is available in: http://openremotesensing.net/knowledgebase/spectral-variability-and-extended-linear-mixing-model/). The data points are assumed to lie in a convex cone spanned by the reference endmembers. The scaling factors, combined with the abundance sum-to-one constraint (ASC) and abundance nonnegativity constraint (ANC), constrain each pixel to lie in a simplex whose vertices are variants of the reference endmembers, situated on straight lines joining the origin and each of the reference endmembers, thus defining the simplex orientation in the cone. In [24], a criterion to perform spectral unmixing using the ELMM is defined in (3), where ψ is the scaling factor rearranged in a $\mathbb{R}^{P \times N}$ matrix and by $\underline{S} = [S_n]$ being $n = 1, \ldots, N$, the collection of pixel-dependent endmember matrices, $A \in \Delta_p$ means that each abundance vector $a_n \in \mathbb{R}^P$ in each pixel belongs to the unit simplex with P vertices, S_0 is a matrix containing reference endmembers, $|| \cdot ||_F$ denotes the Frobenius norm. The term $\lambda_S || S_n - S_0 \psi_n ||_F^2$ forces each endmember to be close (but not equal) to scaled versions of the (unit norm) representatives of the reference directions depending on the value λ_S, which is the regularization parameter on the ELMM tightness. The scaling factors capture illumination-induced variability, while S_n can further consider the intrinsic variability effects. Spatial regularizations incorporate two regularization parameters to tune, $R(A)$ and $R(\psi)$, which are applied to the abundances and the scaling factors, respectively. $R(A)$ is the total variation regularization term on the abundances, promoting smooth abundances while allowing sharp discontinuities when necessary (at the border between objects for instance); $R(\psi)$ is a Tikhonov regularization on the gradient of the abundances to promote spatial smoothness in the scaling factors. They penalize the norm of the spatial gradient of the abundance maps or scaling factors, using the total variation regularization related for the scaling factors and incorporate the constraints
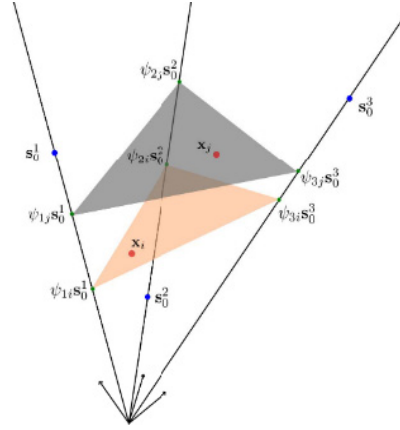

Fig. 2. Geometric interpretation of the ELMM in the case of three endmembers. Red: two data points. Blue: reference endmembers. Green: scaled versions for the two considered pixels [33].

on the variables to enforce spatial smoothing

$$J(A, S, \psi) = \frac{1}{2} \sum_{n=1}^{N} \left(||x_n - S_n a_n||_2^2 + \lambda_S ||S_n - S_0 \psi_k||_F^2 \right) + R(A) + R(\psi). \qquad (3)$$

The data lies in a convex cone whose edges are the endmembers and each pixel belong to a simplex (Fig. 2). However, this formulation relies on the reference endmembers, S_0, and if they are poor representatives of the spectra of the materials, they can cause errors in the estimation of the unmixing parameters. Hence, a new RELMM is proposed [25], which does not rely on the reference endmembers.

D. Robust Extended Linear Mixing Model

RELMM [25] shows endmembers as directions in the feature space, as directional data. The added values of RELMM are the iterative update of S_0 using the volume regularized [39] adapted to a conic model via the unit norm constraints. It allows to iteratively adjust the position of the reference endmember lines in the feature space. Thus, it proposed a new model [25] (4), where tr denotes the trace of a matrix, and $V = P I_P - \mathbb{1}_P \mathbb{1}_P^T$ ($\mathbb{1}_P$, being a column vector of P ones), such that $\mathrm{tr}(S_0 V S_0^T) = \sum_{i=1}^{P-1} \sum_{j=i+1}^{P} ||s_{0i} - s_{0j}||_2^2$. λ_S and λ_{S_0} are the regularization parameters

$$J(A, S, \psi, S_0) = \frac{1}{2} \sum_{n=1}^{N} \left(||x_n - S_n a_n||_2^2 + \lambda_S ||S_n - S_0 \psi_n||_F^2 \right) + \frac{\lambda_{S_0}}{2} \mathrm{tr}\left(S_0 V S_0^T \right) + R(A) + R(\psi). \qquad (4)$$

The fact that the reference endmembers are normalized has also the advantage of easily allowing to compare the magnitude of the scaling factors across different materials and images. Moreover, spatial regularizations [$R(A)$ and $R(\psi)$] can be added as in the ELMM model.

RELMM has the same geometric interpretation as ELMM; however, the reference endmembers in RELMM lie on the unit hypersphere leading to be more accurate than ELMM even when the initialization is poor [25].
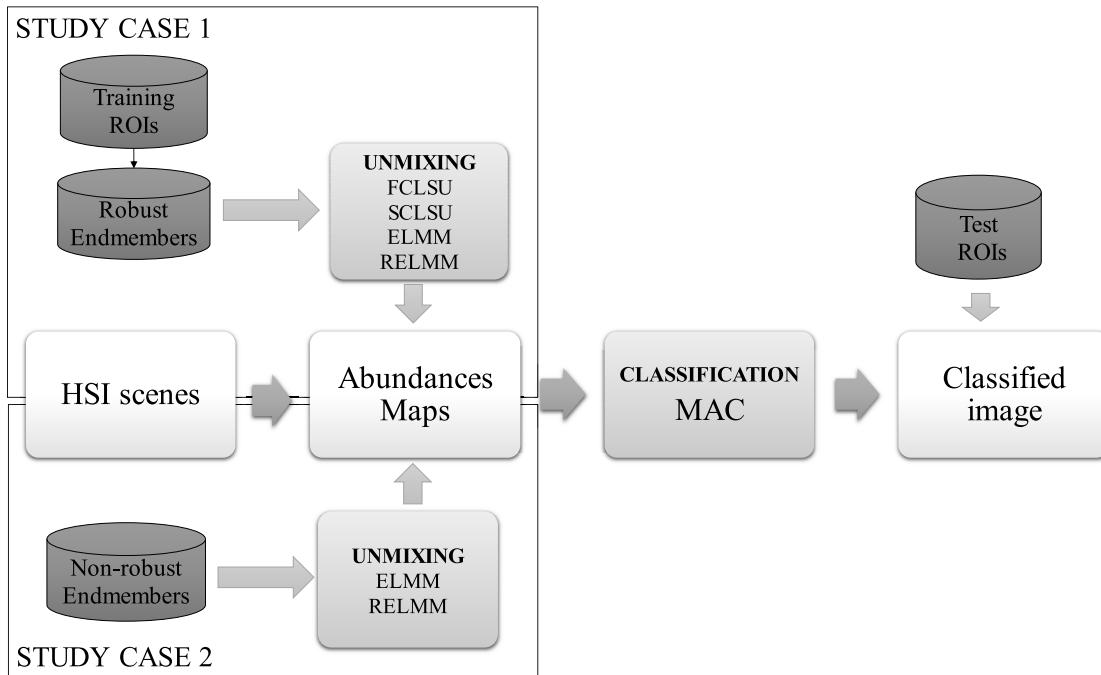
Fig. 3. Flowchart of the unmixing and classification assessment procedure.

IV. METHODOLOGY

A. Study Cases

The analysis can be divided in two different study cases. First, different abundances maps were obtained by FCLSU, SCLSU, ELMM, and RELMM, using robust reference endmembers with many representative pixels for each class under different conditions and, second, using very few nonrobust endmembers (Fig. 3).

For the first part of the study, an extensive field campaign was carried out and the field observation data were acquired to provide accurately located and quantitative ground reference data. Then, regions of interest (ROIs) were manually selected in the original HSI to create accurate training and testing sample sets. Candidate pixels were selected in areas where the vegetation types appeared to be pure and were relatively homogeneous. This procedure was difficult to implement due to the small scale of species spatial distribution and the small size of some vegetation patches. Thus, the samples from the vegetation species mentioned above were identified in the HSI, as well as bare soil and road endmembers. The set of ROIs was divided into a training set to obtain the robust reference endmembers (in average 1400 pixels per class), and the testing set to provide an independent data set to evaluate the classification performances (in average 4500 pixels per class). Robust endmembers used in the first study case were calculated getting the average value of each class for the whole training set of ROIs. Fig. 4 shows the spectral signature of each endmember as well as the picture of each vegetation class. Thus, the robust endmembers used in this section of the study consider every type of spectral variability found in different classes.

In the second part of the study, the performances of ELMM and RELMM are investigated, in order to show the necessity to apply unmixing models, which take the spectral variability into account for obtaining good unmixing results. Thus, non-robust endmembers were acquired getting the average of 1, 3, 5, and 10 pixels per class. They are called nonrobust endmembers because using 1 or 3 pixels for each class, spectral variability is not considered. For instance, nonrobust endmembers obtained from 10 pixels will higher consider spectral variability (its robustness increase) rather than non-robust endmembers obtained from 1 pixel. Thus, it might be seen how ELMM and RELMM models can properly adjust the nonrobust endmembers, allowing to refine and correct those endmembers [25].

B. Methodology Assessment

The quality of the unmixing results can be measured by the reconstruction error calculated by the root-mean-squared error (RMSE) given the set of the original pixels ($x_{\ln_{\text{true}}}$) and the reconstruction data from the corresponding abundances obtained from the pixels and the mixing model ($\hat{x}_{\ln}$). N and L are the given pixel and band, respectively [24], [40] (5)

$$\text{RMSE} = \frac{1}{N} \sum_{n=1}^{N} \sqrt{\frac{1}{L} \sum_{l=1}^{L} \left(x_{\ln_{\text{true}}} - \hat{x}_{\ln} \right)^2} \qquad (5)$$

However, RMSE is an indirect measure, which only shows how the model fits the data, though it is possible to achieve good reconstruction errors with poor abundance and/or spectral variability retrieval. In this context, classification maps were additionally used to assess the methodology. Even though there exists some studies using abundances maps as inputs
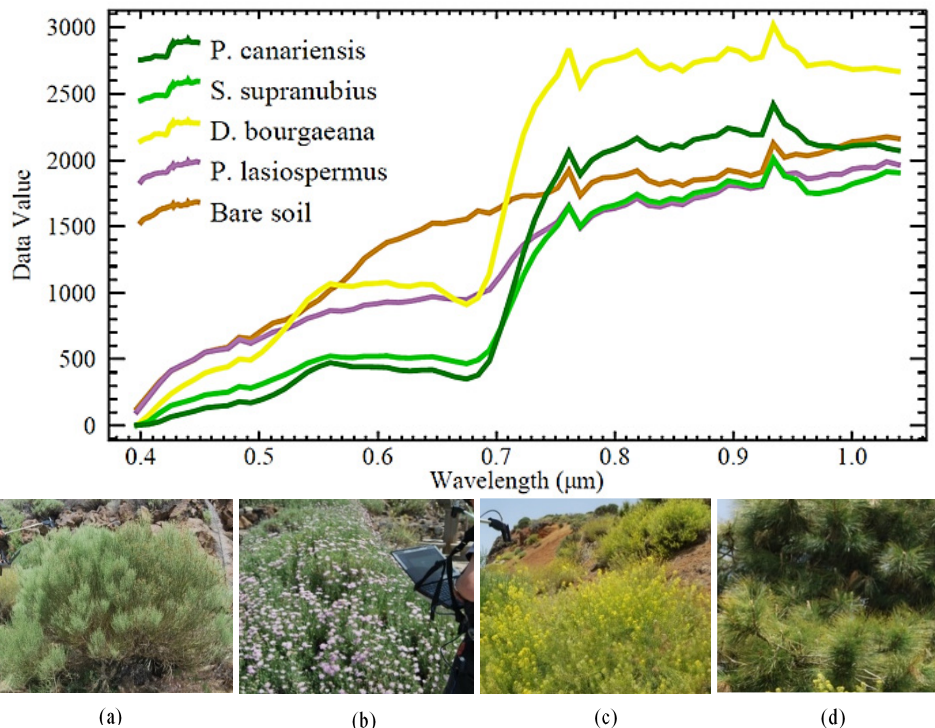
Fig. 4. Endmember spectral signatures used in the study and vegetation of interest. (a) *S. supranubius*. (b) *P. lasiospermus*. (c) *D. bourgaeana*. (d) *P. canariensis*.

for classification [41], [42], classification maps are used as another evaluation process of different unmixing models as well as to solve the hyperdimensionality of the data.

C. HSI Hyperdimensionality Solving Proposal

As dimensionality increases in HSI, more training samples are demanded to obtain thematic maps with higher accuracy. In [10] and [43]–[46], to solve this curse of dimensionality problem, data reduction through band selection or feature extraction reduces dimensionality without the need to increase the number of training samples [43], [47], [48]. Usually, feature extraction and feature selection methods were used by selecting the optimal bands or the optimal subset from the HSI [3]. These techniques significantly reduce the number of suitable components compared to the original dimension [49]. During the past decades, researchers have studied several approaches to alleviate the Hughes phenomenon such as principal component analysis (PCA), minimum noise fraction (MNF), or independent component analysis (ICA). On the other hand, Kernel-based methods, such as support vector machine (SVM), have demonstrated their performance in handling high-dimensional data [50].

Thus, the study proposed to use spectral unmixing models that consider the spectral variability of different classes in order to obtain reasonable abundances maps that will be used for obtaining accurate thematic maps.

In this context, maximum abundance classification (MAC) is proposed, which takes in the abundance maps, the largest abundance vector into the pixel, to set it as a class. Finally, the performance of the classification maps is assessed both

in terms of visual comparisons with general field information on known vegetation structures and using the confusion matrix, whose information is summarized by the overall accuracy (OA) defined as the ratio of the number of validation pixels that are correctly classified to the total number of validation pixels irrespective of the class [51]. In order to obtain the confusion matrices, the testing samples obtained in the first study case were used.

V. RESULTS AND DISCUSSION

This section presents the results of different spectral unmixing methods in different scenes.

The first step was to set the spatial regularization parameters for ELMM and RELMM. Specifically, the values used were $\lambda_S = 0.01$, $\lambda_a = 0.01$, and $\lambda_{psi} = 0.02$, which are the part of S_k, $\mathcal{R}(A)$, and $\mathcal{R}(\psi)$ in (3) and (4), for ELMM and RELMM and $\lambda_{S_0} = 10$, in the RELMM model. They were selected by trial and error, leaving at the beginning λ_a and λ_{psi} at zero, in order to set a suitable λ_S, which is the most crucial parameter to tune. It is observed visually both the abundance and scaling factor maps. A high value of λ_S means that local variants of the endmembers will not drift too far away from the (scaled) reference, whereas a small value means that the local endmembers will get further away from the actual lines. In the last case, the data fit will be better, and the abundance maps will be sparser as a result, since local endmembers will tend to match individual pixels. To get an insight of what happens, scatterplot of the data and local endmembers should be performed, using the first three principal components. Once λ_S is well set up, it is better to choose small λ_a and λ_{psi}
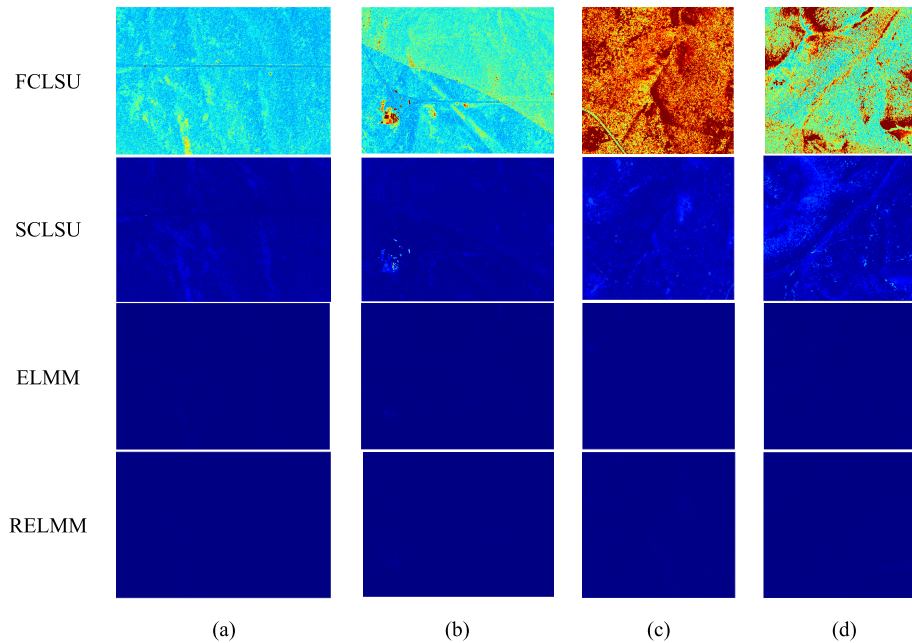
Fig. 5. RMSE maps for FCLSU, SCLSU, ELMM, and RELMM of (a) Area 1, (b) Area 2, (c) Area 3, and (d) Area 4.

TABLE I
RMSE VALUES FOR EACH SCENE USING ROBUST ENDMEMBERS
FOR THE UNMIXING ($\times 10^{-3}$)

	AREA 1	AREA 2	AREA 3	AREA 4
FCLSU	70.21	79.97	183.48	121.65
SCLSU	5.44	5.77	11.37	8.61
ELMM	0.61	0.63	1.09	**0.66**
RELMM	**0.57**	**0.61**	**1.07**	0.72

values. If they look very similar to the ones without the spatial regularizations, the values can be increased. On the other hand, if the abundance maps look too smooth (or even completely uniform), they are way too large and the user could decrease both λ_a and λ_{psi}.

Next, the results of the two study cases are presented.

A. Study Case 1: Spectral Unmixing Using Robust Endmembers

As it was explained in Section III, the study is divided in two study cases. This section shows the results of different spectral unmixing methodologies when the robust endmembers are used as inputs.

Table I shows the average reconstructed RMSE obtained for the four different methods in different scenes (in bold appears the best RMSE value for each scene), whereas Fig. 5 shows the RMSE maps. ELMM and RELMM outperform the FCLSU and SCLSU approaches as it was expected. It can be clearly appreciated the worst accuracy of FCLSU and SCLSU in areas with considerably spectral variation (Areas 2–4) and the good performances of ELMM and RELMM even in such complex scenes. The spatial regularization on the abundances improves the results for ELMM and RELMM, being more robust to noise on the measured data, as well as on the spectral

signatures. The spatial regularization allows to precisely estimate the spatially correlated abundances, removing the noise and the uncertainty that affects to FCLSU and SCLSU [24].

A visual representation of the extracted abundances for Area 2 is shown in Fig. 6. Regarding the abundance maps, every model, except for FCLSU, obtain plausible estimations at visual level. However, most of endmembers are purer for RELMM and ELMM than for SCLSU. The scaling factors extracted by SCLSU, ELMM, and RELMM are displayed in Fig. 7. They show the spectral variation of different classes. As extracting spectral variability is difficult or even impossible when the materials have low abundances, pixels with abundance below 0.5 are removed from the scaling factor maps for a better interpretation. SCLSU scaling factor maps are difficult to interpret as only one scaling factor is estimated for all the endmembers. ELMM and RELMM scaling factor maps show correlation with radiometric and topographic changes, being more evident in *P. lasiospermus* and bare soil maps. In case of Area 2, RELMM gets higher values regarding the radiometric variability due to the sensor pass, being more evident in *P. lasiospermus* map, leading ELMM and RELMM to deal with the induced spectral variability. Again, RELMM obtains higher scaling factor values than ELMM due to its ability to better adjust the references. Therefore, ELMM and RELMM obtain the best results in terms of abundance estimation, as well as spectral variability recovery.

In the case of ELMM and RELMM, the spatial coherency of the abundances and the scaling factors allows to recover the parameters more precisely. In addition, the explicit computation of different scaling factors for each pixel and material allows obtaining sparser variability maps, which also makes ELMM and RELMM stronger in terms of interpretability. Moreover, the spatial regularization parameters of ELMM and RELMM allow to estimate the spatially correlated abundances, removing the noise and the uncertainty, which affects SCLSU,
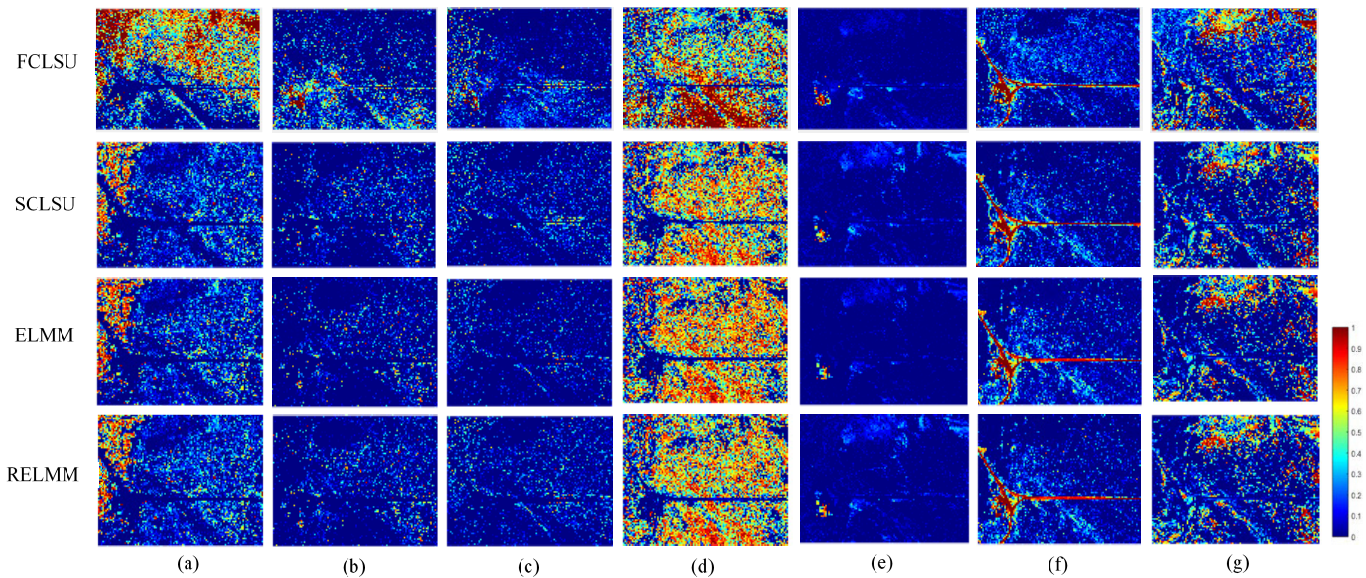
Fig. 6. Abundance maps estimated by FCLSU, SCLSU, ELMM, and RELMM of Area 2. (a) *P. canariensis*. (b) *S. supranubius*. (c) *D. bourgaeana*. (d) *P. lasiospermus*. (e) Urban. (f) Road amd. (g) Bare soil.
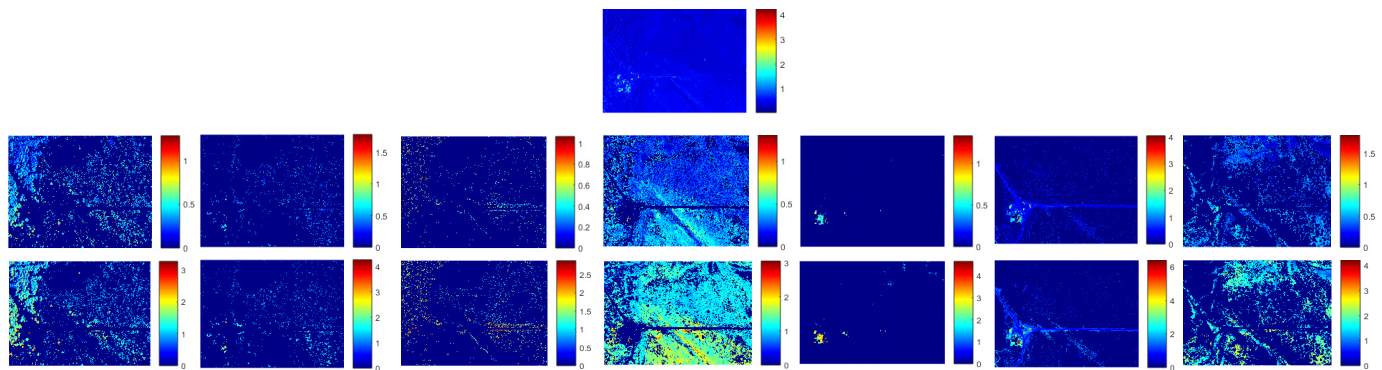

Fig. 7. Scaling factor maps from SCLSU (one scaling factor for all the endmembers), ELMM and RELMM with > 0.5 abundances of Area 2. (a) *P. canariensis*. (b) *S. supranubius*. (c) *D. bourgaeana*. (d) *P. lasiospermus*. (e) Urban. (f) Road. (g) Bare soil.

when two endmember variations of two different materials share a common global shape, and can look quite similar after appropriate scaling [24].

Fig. 8 shows a scatterplot of the data set (in blue) and the endmembers generated by the model (in red) using the first three components of a PCA for Area 2. It can be observed that different materials are equally affected by the spectral variability, being the shape of the variability (red data) or the manifold of the endmember variants, complex. All materials are affected by spectral variability and the conic model advocated by the ELMM and RELMM seems to fit the data. In addition, RELMM scatterplot is sparser than ELMM, meaning that RELMM can adjust the reference and, thus, is able to obtain sparser abundances maps.

Finally, Table II and Fig. 9 show the OA values and the MAC classifications maps obtained from the abundance maps of the unmixing models, respectively. As it was expected, ELMM and RELMM obtain the highest OA, whereas FCLSU obtains the lowest OA. Area 1 shows less difference within the OA obtained from different unmixing models, as this

TABLE II
OA VALUES IN PERCENTAGE (%) RESULTING FROM THE ABUNDANCES MAPS OBTAINED WITH ROBUST ENDMEMBERS

	AREA 1	AREA 2	AREA 3	AREA 4
FCLSU + MAC	76.06	78.81	85.63	64.81
SCLSU + MAC	77.08	86.95	87.43	92.62
ELMM + MAC	77.09	**87.23**	87.82	**92.84**
RELMM + MAC	**78.78**	87.00	**88.18**	92.7

area lacks spectral variability. The difference between the OA values obtained from ELMM and RELMM abundances maps is small (less than 2% in case of Area 1 and less than 0.36% in Areas 2–4). Regarding the classification maps, there is no great visual differences within SCLSU, ELMM, and RELMM, whereas FCLSU classification map clearly shows the radiometric change in the scene, showing how the model does not consider the spectral variability. Regarding the results presented in Fig. 9, some misclassifications can be
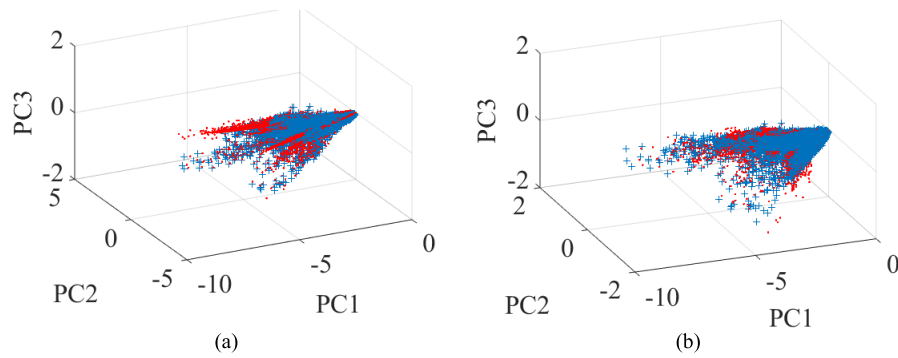
Fig. 8. PCA scatterplot for (a) ELMM and (b) RELMM of Area 2. Blue: data. Red: extracted endmembers.
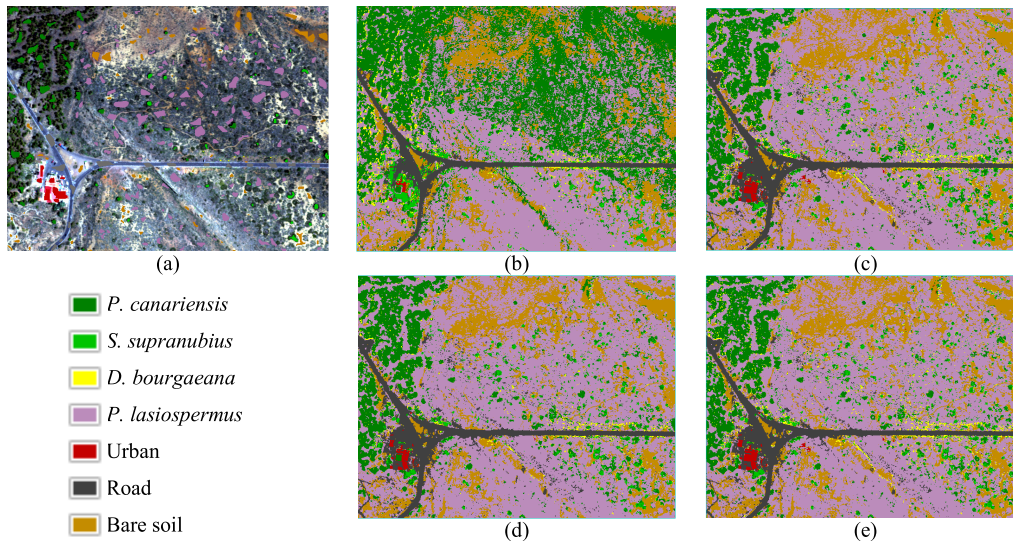

Fig. 9. (a) Ground truth samples and classification maps obtained by (b) FCLSU, (c) SCLSU, (d) ELMM, and (e) RELMM after applying a MAC classification in Area 2.

identified. For instance, some pixels classified as urban (red) or roads (black) appear in bare soil areas. Moreover, in the FCLSU map, *S. supranubius* is incorrectly assigned to urban and road pixels in some areas. Specifically, classes with lower classification accuracy in the four areas analyzed are *S. supranubius* and urban (ca. 60% well classified versus ca. 80% for the remaining classes). Finally, analyzing the (OA%) results, it is obvious how SCLSU, ELMM, and RELMM are considering the spectral variability regarding the blooming of plant individuals.

B. Study Case 2: Spectral Unmixing Using Nonrobust Endmembers

As it was observed in Tables I and II, even though ELMM and RELMM got better results, there is not too much difference between them. Both models consider the spectral variability of endmembers, but if this spectral variability is included in the model by taking many robust endmembers, the robustness of RELMM is not significant. Thus, it seems RELMM will not improve the results much, leading to even slightly worse performance.

In addition, as it is explained in [24], if the abundance of one material is low in a pixel, a different scaling factor for this material will change the orientation of the simplex related to this pixel, but the edge of the simplex, linking the other two (scaled) endmembers, will not change. Hence, the abundance coefficients for the other two materials will not change much either. In this context, both ELMM and RELMM do not require pure pixels to extract the spectral variability of a material efficiently, but only a significant abundance contribution of this material in the considered pixel, or in the neighboring area. Taking this fact into consideration, in this part of the study, nonrobust endmembers were acquired selecting 1, 3, 5, and 10 pixels per class. In this way, the spectral variability is not considered in the endmembers. Since the objective was to observe the robustness of RELMM and ELMM, only both models are included in this study case.

Table III shows the RMSE values for ELMM and RELMM using 1, 3, 5, and 10 pixels to obtain and average endmember for each class. The RMSE values are mostly the same for both methods, except in some cases (Areas 2 and 3), where RELMM got slightly better RMSE. Moreover, the values show a minimum change when more than 1 pixel is taken as reference endmember.

Abundances and scaling factor maps (removing abundances <0.5) for ELMM and RELMM using endmembers from 1 and 10 pixels in Area 4 are shown in Figs. 10 and 11, respectively.
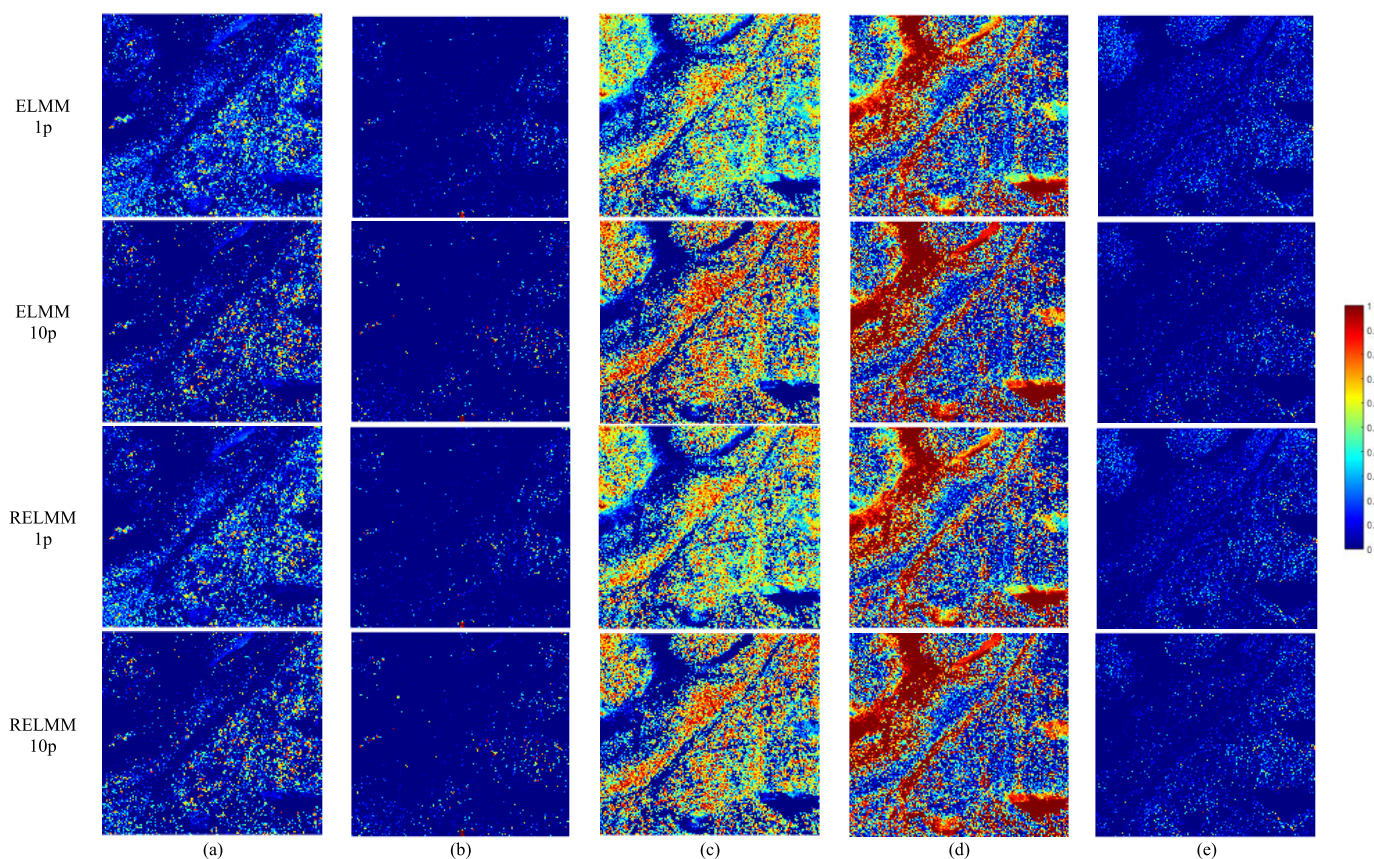
Fig. 10.   Abundance maps estimated in ELMM and RELMM of Area 4 using 1 and 10 pixels for averaging the reference endmembers. (a) *S. supranubius*. (b) *P. canariensis*. (c) *P. laiospermus*. (c) Bare soil. (d)*D. bourgaeana.*
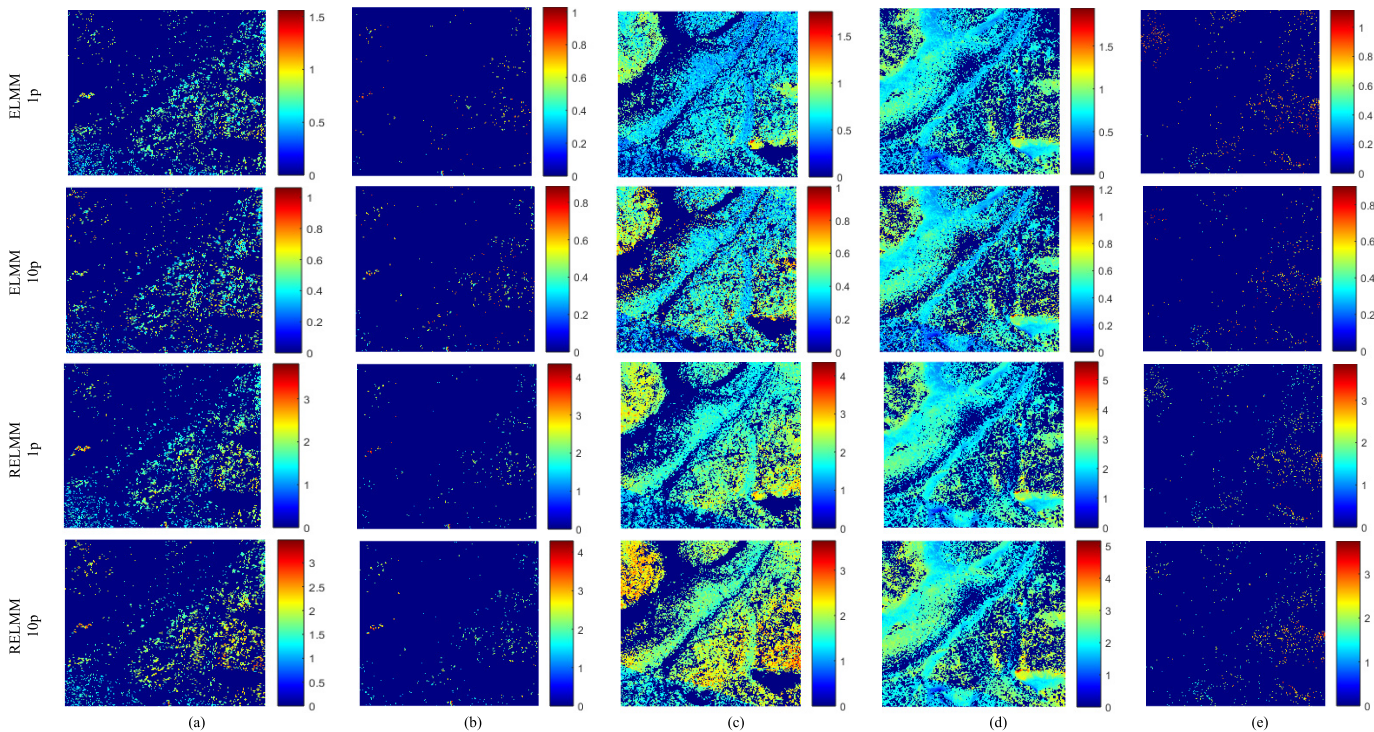

Fig. 11.   Scaling factor maps estimated by ELMM and RELMM in Area 4 using 1 and 10 pixels for averaging the reference endmembers. (a) *S. supranubius*. (b) *P. canariensis*. (c) *P. laiospermus*. (c) Bare soil. (d)*D. bourgaeana.*

It can be observed that even considering 1 or 10 pixels to obtain the reference endmembers, both methods obtain plausible abundances, although abundances values are higher in the case of taking 10 pixels for the reference endmember. Finally, we can assume the good performance of both methods as the radiometric change is solved even taking only 1 pixel for
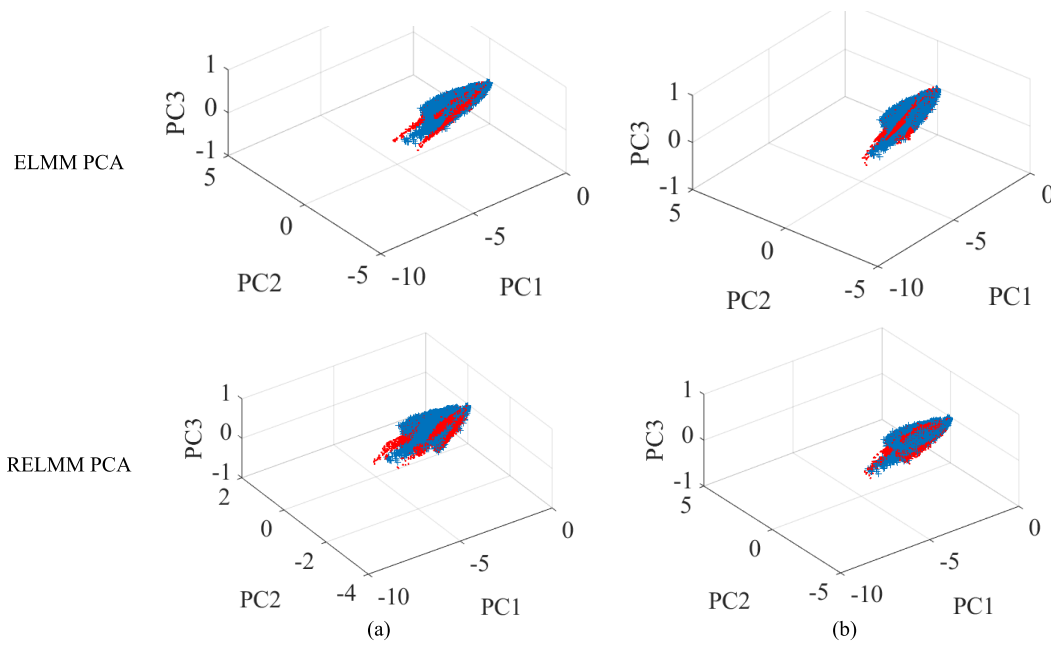
Fig. 12.   PCA scatterplot for ELMM and RELMM of Area 4 using (a) 1 and (b) 10 pixels for averaging the reference endmembers. Blue: data. Red: extracted endmembers.
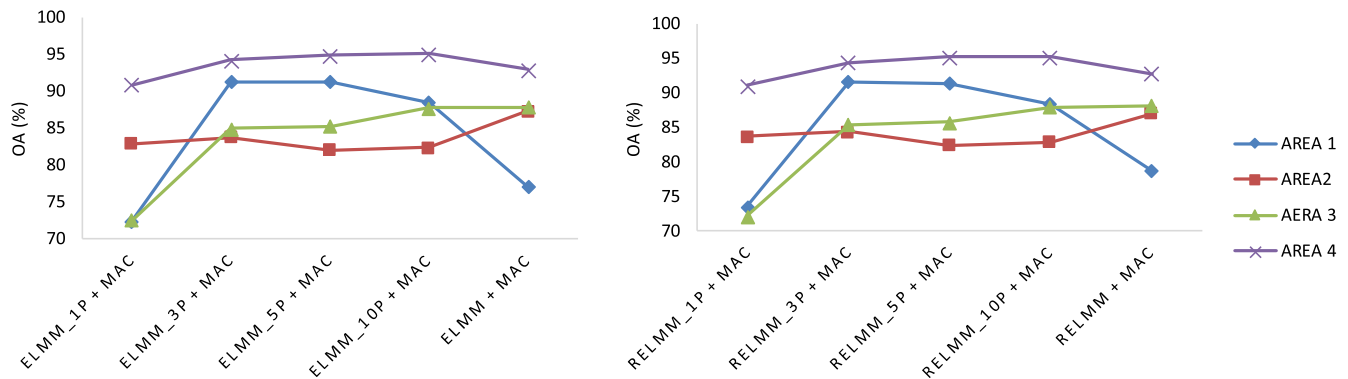

Fig. 13.   OAs results from MAC classification applied to (a) ELMM and (b) RELMM abundances maps from nonrobust to robust endmembers in each area of study.

TABLE III

RMSE VALUES FOR EACH SCENE USING NONROBUST
ENDMEMBERS FOR THE UNMIXING ($\times 10^{-4}$)

	AREA 1	AREA 2	AREA 3	AREA 4
ELMM_1p	7.96	9.80	14.90	**7.87**
RELMM_1p	**7.17**	**7.41**	**13.52**	8.01
ELMM_3p	6.08	7.39	12.14	**7.21**
RELMM_3p	**5.60**	**6.19**	**10.92**	7.45
ELMM_5p	5.73	6.98	11.42	7.61
RELMM_5p	**5.66**	**6.29**	**10.77**	**7.55**
ELMM_10p	5.83	6.67	11.51	**7.26**
RELMM_10p	**5.71**	**6.27**	**10.68**	7.53

endmembers. In this case, *S. supranubius*, *P. lasiospermus*, and bare soil get lower scaling factors in the center of the ravine, as well as in the bottom of the image where sensor swath changes, again, both models have to deal with the induce spectral variability.

The qualitative results of Area 4, using scatterplots of the data in the recovered endmembers of ELMM and RELMM using endmembers obtained from 1 and 10 pixels, are shown in Fig. 12. It is observed how the endmembers in red are close to the edge of the cone defined by the data when the number of averaged endmembers is higher, meaning that they capture more spectral variability. Moreover, RELMM scatterplots are sparser than ELMM, as it occurs in Fig. 8, leading to a better adjustment of the reference endmembers.

OA results obtained from MAC classification are given in Table IV. Accurate classification maps with OA over 70% and achieving values over 84% for the best case depending on the area. Moreover, in most of the cases, RELMM outperforms ELMM. Finally, Fig. 13 shows that classification goodness,

each class and using it as a reference endmember. Regarding the scaling factor maps, it is observed that the values decrease if 10 pixels are considered for the references endmembers, that is, when more spectral variability is taken for the reference

	AREA 1	AREA 2	AREA 3	AREA 4
ELMM_1p + MAC	72.44	82.89	**72.55**	90.86
RELMM_1p + MAC	**73.61**	**83.64**	72.14	**90.99**
ELMM_3p + MAC	91.25	83.68	84.91	94.21
RELMM_3p + MAC	**91.55**	**84.34**	**85.35**	**94.31**
ELMM_5p + MAC	91.29	82.04	85.26	94.86
RELMM_5p + MAC	**92.37**	**82.40**	**85.70**	**95.17**
ELMM_10p + MAC	**88.44**	82.36	87.69	95.06
RELMM_10p + MAC	88.35	**82.85**	**87.93**	**95.11**

using ELMM and RELMM, does not improve when the robustness of the endmembers increases. 3–5 pixels are enough to generate the reference endmembers in order to obtain an accurate classification map.

It is observed how in this part of the study, it is not necessary to get an accurate set of training samples as in the first study case. Only few pixels per class are needed for the spectral unmixing and none for the classification, obtaining accurate classification maps with few knowledge and information of the scene and less effort, avoiding the *Hughes phenomenon*.

VI. CONCLUSION

This paper analyzes different spectral unmixing models: a traditional LMM, the FCLSU, and three models in which the spectral variability as well as the spatial information are considered, SCLSU, assuming a scaling factor that affects equally to all the endmembers present in a pixel, and ELMM and RELMM that assume different scaling factors for each endmembers. The study has been conducted in an ecosystem with high spectral variability within the endmembers due to topography changes, sensor's radiometric change, and an intrinsic spectral variability due to the blooming of plant individuals. In order to evaluate the methods, quantitative results using reconstructed RMSE, as well as classification maps obtained from the abundances maps, are presented.

The analysis has been divided in two different study cases. In the first one, the four models were analyzed by taking a robust set of endmembers that considers the spectral variability of the classes. Regarding the challenge that the ecosystem represents, ELMM and RELMM have shown good performance in terms of abundance estimation and spectral variability retrieval, obtaining a significant lower RMSE than FCLSU and SCSLU and higher OA in the classification. Thus, both models can be successfully applied in images with high spectral variability due to topographic changes but also in images with radiometric differences in each track during the airborne image sensing and the intrinsic spectral variability of plant species blooming, being experimentally confirmed to be well modeled by them.

The second study case proves that ELMM and, specifically, RELMM are useful techniques for obtaining accurate classification maps with both a minimum knowledge of the scene and less effort. Thus, very few pixels were taken to obtain an average reference endmember for each class. In case, this RMSE does not decrease when increasing the endmembers

robustness (from endmembers obtained from 1 to 10 pixels), meaning that increasing the endmembers robustness does not increase the precision of the abundance maps. Moreover, classification maps resulted by taking the abundance maps as inputs, using a hard classification model, RELMM obtains higher OA rather than ELMM, demonstrating that RELMM is more precise in an image with high spectral variability. Thus, the second study case allows analyzing the properties of each pixel, including additional information about the characterization of mixed pixels in the HSI by adding spectral variability. Hence, it proves that RELMM is robust to the absence of pure pixels in the scene, as well as to noise. Moreover, it is confirmed that classification does not improve when the robustness of the endmembers increases. Therefore, it is not necessary a high number of training samples, avoiding the *Hughes phenomenon* by using the abundances maps.

Consequently, an analysis of the endmember variability has been carried out in both study cases, confirming the importance to use unmixing models, which consider the spectral variability. Moreover, it can be concluded from the study, the good performance of the classification maps obtained from the abundance maps, as a tool for evaluating the unmixing models as well as for providing accurate classifications results. Nowadays, obtaining accurate thematic maps are very important in order to study climate changes concerns, population dynamics, anthropogenic pressure, and so on, which are the essential issues for developing ecosystem management plans.

Finally, it would be interesting to test both ELMM and RELMM on other habitats with high heterogeneity and spectral variability. Future research would be devoted to study the spectral variability not only produced by the topographic changes but also by the health status of the species, drought effects, and vegetation canopy. In addition, both models will be analyzed using drone imagery with higher spatial resolution (ca. 10 cm) in which the swath width is narrower and radiometric changes are more evident, as well as the topographic changes and different structures of plant species, i.e., leaves, branches, flowers, and shadows.

REFERENCES

[1] C. A. Mücher, L. Kooistra, M. Vermeulen, J. V. Borre, B. Haest, and R. Haveman, "Quantifying structure of natura 2000 heathland habitats using spectral mixture analysis and segmentation techniques on hyperspectral imagery," *Ecological Indicators*, vol. 33, pp. 71–81, Oct. 2013.

[2] S. Delalieux, B. Somers, B. Haest, T. Spanhove, J. V. Borre, and C. A. Mücher, "Heathland conservation status mapping through integration of hyperspectral mixture analysis and decision tree classifiers," *Remote Sens. Environ.*, vol. 126, pp. 222–231, Nov. 2012.

[3] Y. Dian, Z. Li, and Y. Pang, "Spectral and texture features combined for forest tree species classification with airborne hyperspectral imagery," *J. Indian Soc. Remote Sens.*, vol. 43, pp. 101–107, Mar. 2015.

[4] L. Ballanti, L. Blesius, E. Hines, and B. Kruse, "Tree species classification using hyperspectral imagery: A comparison of two classifiers," *Remote Sens.*, vol. 8, p. 445, May 2016.

[5] J. M. Bioucas-Dias *et al.*, "Hyperspectral unmixing overview: Geometrical, statistical, and sparse regression-based approaches," *IEEE J. Sel. Topics Appl. Earth Observ. Remote Sens.*, vol. 5, no. 2, pp. 354–379, Apr. 2012.

[6] P.-A. Thouvenin, N. Dobigeon, and J.-Y. Tourneret, "Hyperspectral unmixing with spectral variability using a perturbed linear mixing model," *IEEE Trans. Signal Process.*, vol. 64, no. 2, pp. 525–538, Jan. 2016.

[7] I. G. Dópido, "New techniques for hyperspectral image classification," Ph.D. dissertation Dept. Tecnología de los computadores las comunicaciones, Universidad de Extremadura, Badajoz, Spain, 2013.

[8] M. Fauvel, Y. Tarabalka, J. A. Benediktsson, J. Chanussot, and J. C. Tilton, "Advances in spectral-spatial classification of hyperspectral images," *Proc. IEEE*, vol. 101, no. 3, pp. 652–675, Mar. 2013.

[9] G. Camps-Valls, D. Tuia, L. Bruzzone, and J. A. Benediktsson, "Advances in hyperspectral image classification: Earth monitoring with statistical learning methods," *IEEE Signal Process. Mag.*, vol. 31, no. 1, pp. 45–54, Jan. 2014.

[10] P. Ghamisi, J. Plaza, Y. Chen, J. Li, and A. J. Plaza, "Advanced spectral classifiers for hyperspectral images: A review," *IEEE Geosci. Remote Sens. Mag.*, vol. 5, no. 1, pp. 8–32, Mar. 2017.

[11] A. Villa, J. Chanussot, C. Jutten, J. A. Benediktsson, and S. Moussaoui, "On the use of ICA for hyperspectral image analysis," in *Proc. IEEE Int. Geosci. Remote Sens. Symp.*, Jul. 2009, pp. IV97–IV100.

[12] G. Hughes, "On the mean accuracy of statistical pattern recognizers," *IEEE Trans. Inf. Theory*, vol. IT-14, no. 1, pp. 55–63, Jan. 1968.

[13] P. Ghamisi, J. A. Benediktsson, and S. Phinn, "Land-cover classification using both hyperspectral and LiDAR data," *Int. J. Image Data Fusion*, vol. 6, no. 3, pp. 189–215, 2015.

[14] N. Keshava and J. F. Mustard, "Spectral unmixing," *IEEE Signal Process. Mag.*, vol. 19, no. 1, pp. 44–57, Jan. 2002.

[15] E. L. Hestir *et al.*, "Identification of invasive vegetation using hyperspectral remote sensing in the california delta ecosystem," *Remote Sens. Environ.*, vol. 112, pp. 4034–4047, Nov. 2008.

[16] C. Zhang, "Applying data fusion techniques for benthic habitat mapping and monitoring in a coral reef ecosystem," *ISPRS J. Photogramm. Remote Sens.*, vol. 104, pp. 213–223, Jun. 2015.

[17] M. Garcia and S. L. Ustin, "Detection of interannual vegetation responses to climatic variability using AVIRIS data in a coastal savanna in California," *IEEE Trans. Geosci. Remote Sens.*, vol. 39, no. 7, pp. 1480–1490, Jul. 2001.

[18] B. Hapke, *Theory of Reflectance and Emittance Spectroscopy*. Cambridge, U.K.: Cambridge Univ. Press, 2012.

[19] M. A. Veganzones *et al.*, "A new extended linear mixing model to address spectral variability," in *Proc. 6th Workshop Hyperspectral Image Signal Process. Evol. Remote Sens. (WHISPERS)*, Jun. 2014, pp. 1–4.

[20] B. Somers, G. P. Asner, L. Tits, and P. Coppin, "Endmember variability in spectral mixture analysis: A review.," *Remote Sens. Environ.*, vol. 115, pp. 1603–1616, Jul. 2011.

[21] A. Zare and K. Ho, "Endmember variability in hyperspectral analysis: Addressing spectral variability during spectral unmixing," *IEEE Signal Process. Mag.*, vol. 31, no. 1, pp. 95–104, Jan. 2014.

[22] X. Zhang, J. Zhang, C. Li, C. Cheng, L. Jiao, and H. Zhou, "Hybrid unmixing based on adaptive region segmentation for hyperspectral imagery," *IEEE Trans. Geosci. Remote Sens.*, vol. 56, no. 7, pp. 3861–3875, Jul. 2018.

[23] C. L. Lawson and R. J. Hanson, *Solving Least Squares Problems*. Philadelphia, PA, USA: SIAM, 1995.

[24] L. Drumetz, M.-A. Veganzones, S. Henrot, R. Phlypo, J. Chanussot, and C. Jutten, "Blind hyperspectral unmixing using an extended linear mixing model to address spectral variability," *IEEE Trans. Image Process.*, vol. 25, no. 8, pp. 3890–3905, Aug. 2016.

[25] L. Drumetz, J. Chanussot, and A. Iwasaki, "Endmembers as directional data for robust material variability retrieval in hyperspectral image unmixing," in *Proc. IEEE Int. Conf. Acoust. Speech Signal Process. (ICASSP)*, Apr. 2018, pp. 3404–3408.

[26] N. González-Lemus, J. C. Carracedo-Gómez, and M. D. Villonga, "El parque nacional del Teide: Patrionio mundial de la UNESCO," *Anuario Estudios Atlánticos*, vol. 55, pp. 519–568, 2009.

[27] V. Garzón-Machado, M. J. D. Arco-Aguilar, and P.-L. Pérez-de-Paz, "A tool set for description and mapping vegetation on protected natural areas: An example from the canary islands," *Biodiversity Conservation*, vol. 20, pp. 3605–3625, Dec. 2011.

[28] J. Cubas *et al.*, "Contrasting effects of invasive rabbits on endemic plants driving vegetation change in a subtropical alpine insular environment," *Biol. Invasions*, vol. 20, pp. 793–807, Mar. 2018.

[29] E. de Miguel *et al.*, "The processing of CASI-1500I data at INTA PAF," *EARSeL eProc.*, vol. 13, no. 1, pp. 30–37, 2014.

[30] R. B. Singer and T. B. McCord, "Mars—Large scale mixing of bright and dark surface materials and implications for analysis of spectral reflectance," in *Proc. Lunar Planet. Sci. Conf.*, 1979, pp. 1835–1848.

[31] D. B. Nash and J. E. Conel, "Spectral reflectance systematics for mixtures of powdered hypersthene, labradorite, and ilmenite," *J. Geophys. Res.*, vol. 79, pp. 1615–1621, Apr. 1974.

[32] D. C. Heinz and C.-I. Chang, "Fully constrained least squares linear spectral mixture analysis method for material quantification in hyperspectral imagery," *IEEE Trans. Geosci. Remote Sens.*, vol. 39, no. 3, pp. 529–545, Mar. 2001.

[33] S. Henrot, J. Chanussot, and C. Jutten, "Correction to 'dynamical spectral unmixing of multitemporal hyperspectral images' [Jul 16 3219–3232]," *IEEE Trans. Image Process.*, vol. 25, no. 9, p. 4443, Sep. 2016.

[34] C. A. Bateson, G. P. Asner, and C. A. Wessman, "Endmember bundles: A new approach to incorporating endmember variability into spectral mixture analysis," *IEEE Trans. Geosci. Remote Sens.*, vol. 38, no. 2, pp. 1083–1094, Mar. 2000.

[35] B. Somers, M. Zortea, A. Plaza, and G. Asner, "Automated extraction of image-based endmember bundles for improved spectral unmixing," *IEEE J. Sel. Topics Appl. Earth Observat. Remote Sens.*, vol. 5, no. 2, pp. 396–408, Apr. 2012.

[36] D. A. Roberts, M. Gardner, R. Church, S. Ustin, G. Scheer, and R. O. Green, "Mapping chaparral in the Santa Monica Mountains using multiple endmember spectral mixture models," *Remote Sens. Environ.*, vol. 65, no. 3, pp. 267–279, Sep. 1998.

[37] G. P. Asner and D. B. Lobell, "A biogeophysical approach for automated SWIR unmixing of soils and vegetation," *Remote Sens. Environ.*, vol. 74, no. 1, pp. 99–112, Oct. 2000.

[38] L. Drumetz, "Endmember variability in hyperspectral image unmixing," Ph.D. dissertation, Univ. Grenoble Alpes, Grenoble, France, 2016.

[39] M. Berman, H. Kiiveri, R. Lagerstrom, A. Ernst, R. Dunne, and J. F. Huntington, "ICE: A statistical approach to identifying endmembers in hyperspectral images," *IEEE Trans. Geosci. Remote Sens.*, vol. 42, no. 10, pp. 2085–2095, Oct. 2004. doi: 10.1109/TGRS.2004.835299.

[40] M. A. Veganzones, G. Tochon, M. Dalla-Mura, A. J. Plaza, and J. Chanussot, "Hyperspectral image segmentation using a new spectral unmixing-based binary partition tree representation," *IEEE Trans. Image Process.*, vol. 23, no. 8, pp. 3574–3589, Aug. 2014.

[41] J. Sigurdsson, M. O. Ulfarsson, and J. R. Sveinsson, "Total variation and ℓqbased hyperspectral unmixing for feature extraction and classification," in *Proc. IEEE Int. Geosci. Remote Sens. Symp. (IGARSS)*, Jul. 2015, pp. 437–440.

[42] A. M. Machín, J. Marcello, A. I. Hernández-Cordero, J. M. Abasolo, and F. Eugenio, "Vegetation species mapping in a coastal-dune ecosystem using high resolution satellite imagery," *GIsci. Remote Sens.*, vol. 56, no. 2, pp. 210–232, 2018.

[43] F. E. Fassnacht *et al.*, "Comparison of feature reduction algorithms for classifying tree species with hyperspectral data on three central european test sites," *IEEE J. Sel. Topics Appl. Earth Observ. Remote Sens.*, vol. 7, no. 6, pp. 2547–2561, Jun. 2014.

[44] G. A. Licciardi and F. D. Frate, "A comparison of feature extraction methodologies applied on hyperspectral data," in *Proc. Hyperspectral, Workshop*, Frascati, Italy, 2010, pp. 17–19.

[45] L. Wang and C. Zhao, *Hyperspectral Image Processing*. Springer, 2016. doi: 10.1109/MGRS.2013.2244672.

[46] J. M. Bioucas-Dias, A. Plaza, G. Camps-Valls, P. Scheunders, N. M. Nasrabadi, and J. Chanussot, "Hyperspectral remote sensing data analysis and future challenges," *IEEE Geosci. Remote Sens. Mag.*, vol. 1, no. 2, pp. 6–36, Jun. 2013.

[47] M. L. Clark, D. A. Roberts, and D. B. Clark, "Hyperspectral discrimination of tropical rain forest tree species at leaf to crown scales," *Remote Sens. Environ.*, vol. 96, pp. 375–398, Jun. 2005.

[48] C. Li, J. Yin, and J. Zhao, "Using improved ICA method for hyperspectral data classification," *Arabian J. Sci. Eng.*, vol. 39, no. 1, pp. 181–189, 2014.

[49] J. Ren, J. Zabalza, S. Marshall, and J. Zheng, "Effective feature extraction and data reduction in remote sensing using hyperspectral imaging [applications corner]," *IEEE Signal Process. Mag.*, vol. 31, no. 4, pp. 149–154, Jul. 2014.

[50] G. Camps-Valls and L. Bruzzone, "Kernel-based methods for hyperspectral image classification," *IEEE Trans. Geosci. Remote Sens.*, vol. 43, no. 6, pp. 1351–1362, Jun. 2005.

[51] E. Belluco *et al.*, "Mapping salt-marsh vegetation by multispectral and hyperspectral remote sensing," *Remote Sens. Environ.*, vol. 105, pp. 54–67, Nov. 2006.

Edurne Ibarrola-Ulzurrun received the B.S. degree in biology from the University of Navarra, Pamplona, Spain, in 2011, and the M.S. degree in plant ecology and remote sensing from the University of Tromsø, Tromsø, Norway, in 2014. She is currently pursuing the Ph.D. degree in oceanography and global change with the Institute of Oceanography and Global Change (IOCAG), University of Las Palmas de Gran Canaria (ULPGC), Spain.

She has authored three articles and a chapter book. Her Ph.D. interest is about advanced processing of remote sensing data for the monitoring and sustainable management terrestrial resources in vulnerable systems, especially remote sensing image processing, both multispectral and hyperpsespectral imagery, preprocessing, such as pansharpening, hyperspectral dimensionality reduction, and so on, pixel and object classification, spectral unmixing, as well as, plant ecology and environmental management.

Ms. Ibarrola-Ulzurrun was a recipient of the Best Student Paper Award in SPIE Remote Sensing International Conference 2016.

Lucas Drumetz (M'17) received the M.Sc. degree in electrical engineering from the Grenoble Institute of Technology (Grenoble INP), Grenoble, France, in 2013, and the Ph.D. degree from the Université de Grenoble Alpes, Grenoble, in 2016.

In 2017, he was a Visiting Assistant Professor with the University of California at Los Angeles (UCLA), Los Angeles, CA, USA. In 2017, he was a Visiting Researcher with the University of Tokyo, Tokyo, Japan. Since 2018, he has been an Associate Professor with the Department of Signal and Communications, IMT-Atlantique, Brest, France. His research interests include signal and image processing, inverse problems, optimization techniques and machine learning for remote sensing data.

Dr. Drumetz received the 2017 Best Ph.D. Award from the Université de Grenoble Alpes.

Javier Marcello (M'99–SM'12) received the M.S. degree in electrical engineering from the Technical University of Catalonia (UPC), Barcelona, Spain, in 1993, and the Ph.D. degree from the Universidad de Las Palmas de Gran Canaria (ULPGC), Las Palmas de Gran Canaria, Spain, in 2006.

From 1992 to 2000, he was the Head Engineer of the Spanish Aerospace Defense Administration, Instituto Nacional de Técnica Aeroespacial, Canary Space Center, San Bartolomé de Tirajana, Gran Canaria, for different programs (Cospas-Sarsat, MINISAT, Helios, and CREPAD). In 1994, he joined the Department of Signal and Communications, ULPGC, where he has been an Associate Professor with the Telecommunication School, lecturing on the areas of satellite and radio communications, since 2000. His research is carried out at the Institute of Oceanography and Global Change (IOCAG), ULPGC, which includes multisensor remote sensing image processing (image fusion, classification, and segmentation) and the generation of coastal and land products. He has authored many papers in indexed remote sensing journals and reviewer in more than 20 remote publications.

Dr. Marcello has been the Vice-President of the IEEE Geoscience and Remote Sensing Spanish Chapter since 2016.

Consuelo Gonzalo-Martín received the B.A. degree in physics from Salamanca University, Salamanca, Spain, and the Ph.D. degree in physics from the Complutense University of Madrid, Madrid, Spain, in 1986 and 1989, respectively.

Since 1993, she has been with the Department of Architecture and Technology of Computers, Computer School, Universidad Politécnica de Madrid, Madrid, Spain. Since 2012, she has been a member of the MIDAS (Data Mining and Simulation) Research Group, Center for Biomedical Technology, Technical University of Madrid (UPM), Madrid. Her main contributions have been in the areas of image processing through digital and optical implementations of joint representations, as well as the development of new artificial neural networks algorithms. The fields of application have been primarily remote sensing, medical imaging, and recognition of faces. In particular, in the area of remote sensing is coauthor of new algorithms for merging optical satellite image. At present, her main line of research is the proposal of new methodologies for image analysis based on objects (OBIA) for both classification and automatic interpretation of satellite images as medical. Also, she is involved in research and development projects for text and image mining in the health care domain. As a result of her research, she has directed more than 15 financed research projects and participated in around 20 more. She has coauthored 38 international journal publications, most of them with high impact factor in the remote sensing area and has participated in most of 50 international congresses.

Jocelyn Chanussot (M'04–SM'04–F'12) received the M.Sc. degree in electrical engineering from the Grenoble Institute of Technology (Grenoble INP), Grenoble, France, in 1995, and the Ph.D. degree from the Université de Savoie, Annecy, France, in 1998.

In 1999, he was with the Geography Imagery Perception Laboratory for the Delegation Generale de l'Armement (DGA—French National Defense Department), Arcueil, France. From 2015 to 2017, he was a Visiting Professor with the University of California at Los Angeles (UCLA), Los Angeles, CA, USA. Since 1999, he has been with Grenoble INP, where he is currently a Professor of signal and image processing. He is also conducting his research at the Grenoble Images Speech Signals and Automatics Laboratory (GIPSA-Lab). He has been a Visiting Scholar with Stanford University, Stanford, CA, USA; KTH Royal Institute of Technology, Stockholm, Sweden; and National University of Singapore, Singapore. Since 2013, he has been an Adjunct Professor with the University of Iceland, Reykjavik, Iceland. His research interests include image analysis, multicomponent image processing, nonlinear filtering, and data fusion in remote sensing.

Dr. Chanussot was a member of the IEEE Geoscience and Remote Sensing Society AdCom from 2009 to 2010, in charge of membership development, the Machine Learning for Signal Processing Technical Committee of the IEEE Signal Processing Society from 2006 to 2008, and the Institut Universitaire de France from 2012 to 2017. He is the Founding President of the IEEE Geoscience and Remote Sensing French Chapter from 2007 to 2010 which received the 2010 IEEE GRS-S Chapter Excellence Award. He was a co-recipient of the NORSIG 2006 Best Student Paper Award, the IEEE GRSS 2011 and 2015 Symposium Best Paper Award, the IEEE GRSS 2012 Transactions Prize Paper Award, and the IEEE GRSS 2013 Highest Impact Paper Award. He was the General Chair of the first IEEE GRSS Workshop on Hyperspectral Image and Signal Processing, Evolution in Remote sensing (WHISPERS). He was the Chair from 2009 to 2011 and the Co-Chair of the GRS Data Fusion Technical Committee from 2005 to 2008. He was the Program Chair of the IEEE International Workshop on Machine Learning for Signal Processing, (2009). He served as an Associate Editor for IEEE GEOSCIENCE AND REMOTE SENSING LETTERS from 2005 to 2007 and *Pattern Recognition* from 2006 to 2008. Since 2007, he has an Associate Editor for the IEEE TRANSACTIONS ON GEOSCIENCE AND REMOTE SENSING. He was a Guest Editor for the Proceedings of the IEEE in 2013 and the *IEEE Signal Processing Magazine* in 2014. He was the Editor-in-Chief of the *IEEE Journal of Selected Topics in Applied Earth Observations and Remote Sensing* from 2011 to 2015.